

Formation of globular clusters induced by external ultraviolet radiation

Kenji Hasegawa^{1*}, Masayuki Umemura¹ and Tetsu Kitayama² *

¹Centre for Computational Sciences, University of Tsukuba, Ten-nodai, 1-1-1 Tsukuba, Ibaraki 305-8577, Japan

²Department of Physics, Toho University, Funabashi, Chiba 274-8510, Japan

Accepted 2009 May 7. Received 2009 May 1; in original form 2008 July 3

ABSTRACT

We present a novel scenario for globular cluster (GC) formation, where the ultraviolet (UV) background radiation effectively works so as to produce compact star clusters. Recent observations on the age distributions of GCs indicate that many GCs formed even after the cosmic reionization epoch. This implies that a significant fraction of GCs formed in UV background radiation fields. Also, the star formation in an early-generation of subgalactic objects may be affected by strong UV radiation from preformed massive stars, e.g., Population III stars. Here, we explore the formation of GCs in UV radiation fields. For this purpose, we calculate baryon and dark matter (DM) dynamics in spherical symmetry, incorporating the self-shielding effects by solving the radiative transfer of UV radiation. In addition, we prescribe the star formation in cooled gas components and pursue the dynamics of formed stars. As a result, we find that the evolution of subgalactic objects in UV background radiation are separated into three types, that is, (1) *prompt star formation*, where less massive clouds ($\sim 10^{5-8}M_{\odot}$) are promptly self-shielded and undergo star formation, (2) *delayed star formation*, where photoionized massive clouds ($\gtrsim 10^8M_{\odot}$) collapse despite high thermal pressure and are eventually self-shielded to form stars in a delayed fashion, and (3) *supersonic infall*, where photoionized less massive clouds ($\sim 10^{5-8}M_{\odot}$) contract with supersonic infall velocity and are self-shielded when a compact core forms. In particular, the type (3) is a novel type found in the present simulations, and eventually produces a very compact star cluster. The resultant mass-to-light ratios, half-mass radii, and velocity dispersions for the three types are compared to the observations of GCs, dwarf spheroidals (dSphs), and ultra-compact dwarfs (UCDs). It turns out that the properties of star clusters resulting from *supersonic infall* match well with those of observed GCs, whereas the other two types are distinct from GCs. Hence, we conclude that *supersonic infall* in a UV background is a promising mechanism to form GCs.

Key words: galaxies: formation - globular clusters: general - galaxies: dwarf - radiative transfer - hydrodynamics

1 INTRODUCTION

Globular clusters (GCs) are characterized by their compactness, old age, and low metallicity. Although the mass range of GCs ($10^{5-6}M_{\odot}$) is similar to that of dwarf spheroidal galaxies (dSphs), GCs have much higher stellar velocity dispersions than those of dSphs. In addition, the velocity dispersions in GCs correlate with their luminosities in a definitely different fashion from that in dSphs. Furthermore, the survey of Fornax galaxy cluster has revealed a new

class of dwarf galaxies, that is, ultra compact dwarf galaxies (UCDs), which are more compact than normal dwarf galaxies but clearly distinct from GCs (Drinkwater et al. 2003). According to the virial theorem, the velocity dispersion is expressed as $\sigma_* \propto \sqrt{GM/r_h}$, where M and r_h are the total mass and the half-mass radius of a system. The velocity dispersion is then related to the luminosity by $\sigma_* \propto L^{1/3}$, assuming $M \propto r_h^3$ and $L \propto M$. Observed GCs, however, show the correlation like $\sigma_* \propto L^{1/2}$ (Djorgovski et al. 1997; McLaughlin & van der Marel 2005). This correlation can be derived if GC radii are almost independent of mass (Ashman & Zepf 2001). Interestingly, such a correlation is found not only in Galactic GCs but also in GCs in external galaxies (Hasegan et al. 2005).

* E-mail: hasegawa@ccs.tsukuba.ac.jp (KH);
umemura@ccs.tsukuba.ac.jp (MU); kitayama@ph.sci.toho-u.ac.jp (TK)

Also, the $\sigma_* - L$ relation of UCDs obviously deviates from the virial theorem (Drinkwater et al. 2003). As for dSphs, some follow $\sigma_* \propto L^{1/3}$, but the majority of dSphs show higher velocity dispersions than expected with the virial theorem (Mateo 1998; Matin et al. 2006; Simon & Geha 2007; McConnachie & Irwin 2006; Majewski et al. 2007). These imply that GCs as well as UCDs and many dSphs did not form through simple gravitational collapse and virialization.

Various scenarios for the formation GCs have been hitherto considered by many authors (e.g., Peebles & Dicke 1968; Fall & Rees 1985; Ashman & Zepf 1992; Murray & Lin 1992; Bromm & Clarke 2002; Kravtsov & Gnedin. 2005; Saitoh et al. 2006). They are mainly divided into three categories, based on the formation epoch of GCs relative to that of a host galaxy. The first one is a merger scenario, in which GCs form in the gas-rich mergers of disk galaxies (Ashman & Zepf 1992). In this scenario, interstellar gas is highly compressed by shocks induced by the mergers, and very compact star clusters are expected to form. Such events likely occur at a later stage of galaxy formation, therefore formed star clusters would be young. This scenario can explain young star clusters observed in merging or starbursting galaxies. However, it might be difficult to explain old GC populations. Moreover, the metallicity of star clusters is expected to be the same as that of merging galaxies, which may be higher than the GC metallicity of $Z \simeq 10^{-4} - 10^{-2} Z_\odot$.

In the second scenario, GCs form at the early stage of the host galaxy evolution. Fall & Rees (1985) firstly have shown the possibility of GCs formation caused by thermal instability, in which proto-globular clusters are formed from dense gas clouds with $T \sim 10^4$ K confined by diffuse hot gas with $T \sim 10^6$ K. In this case, the Jeans mass for such dense clouds roughly corresponds to the typical mass scale for observed GCs ($10^{5-6} M_\odot$). In this model, the clouds should be metal-poor to maintain the cloud temperature as $T \sim 10^4$ K. A similar idea have been explored by Murray & Lin (1992), in which the temperature of dense clouds is maintained as $T \sim 10^4$ K by photoheating. Kravtsov & Gnedin. (2005) have carried out high resolution simulations, and shown that GCs can form in high-density cores of giant molecular clouds in dense gaseous disk of galaxies. They also have found that the resultant ratio of the total GC mass to the baryonic mass of the host galaxy is as small as $\approx 10^{-4}$, as indicated by observations (McLaughlin 1999).

The last one is the pregalactic formation scenario that has been widely explored, in which GCs form in dark matter (DM) minihaloes before they infall into galactic haloes. This is a plausible scenario for the formation of low-mass star clusters, and it can account for many properties of GCs such as low metallicity and old age comparable to the cosmic age (e.g., Bromm & Clarke 2002; Mashchenko & Sills 2005; Saitoh et al. 2006). However, proto-GCs in this scenario are expected to be dominated by dark matter (DM), and possess the mass-to-light ratios of $M/L \sim 10$. Therefore, it does not provide a direct explanation for observed GCs that have mass-to-light ratios as low as $M/L \sim 1$ (Pryor & Meylan 1993). Recent simulations of galaxy formation by Saitoh et al. (2006) have indicated that diffuse DM haloes are selectively stripped by tidal interactions with their host galaxy, and baryon-dominated star clusters are naturally explained. However, the spatial resolution of the

simulations cannot allow us to discuss the internal structure of proto-globular clouds. Therefore, the physical reason for condensations of the proto-globular clouds is still uncertain. The stripping of DM haloes also has been studied using N -body calculations by Mashchenko & Sills (2005), where a hybrid cluster composed of stars and DM is simulated in the external tidal field of the host galaxy. They assumed initially a compact baryon core embedded in a diffuse DM halo, and explored the dynamical evolution using N -body simulations. They have found that the surface brightness profiles and mass-to-light ratios for the evolved hybrid GCs are consistent with those of observed GCs. However, it has not been clarified yet how such compact stellar systems form at first. Since the virial radii of collapsed objects at $z \sim 10$ are several hundred parsecs in the mass range of $10^{5-6} M_\odot$, that are $\sim 10 - 100$ times larger than the sizes of observed GCs. Hence it is not easy to form baryon-dominated star clusters. An additional physical mechanism seems to be requisite to produce a compact stellar core. Moreover, for all the above scenarios, the physical mechanism to explain the $\sigma_* - L$ relation of GCs has not been elucidated.

The ages of Galactic GCs show a broad distribution with the mean age of about 12.3 Gyr (Puzia, Perrett & Bridges 2005). A significant fraction of GCs seem to form after the cosmic reionization epoch $z_r \simeq 11$, which is inferred by *Wilkinson Microwave Anisotropic Probe* (WMAP) three year data (Page et al. 2007) and five year data (Komatsu et al. 2009). Therefore, not a few GCs are thought to form in UV background radiation fields. Also, the formation of GCs itself might contribute much to the reionization of the universe at redshift $z \approx 6$ (Ricotti 2002). Furthermore, even before the reionization, the star formation in an early-generation of galaxies can be affected by strong UV radiation from preformed massive stars including Population III (Pop III) stars. Thus, it is of great significance to consider the formation of GCs in UV radiation fields. When a gas cloud is photo-ionized, the cloud is heated up to $\sim 10^4$ K (Umemura & Ikeuchi 1984; Thoul & Weinberg 1996). In addition, soft UV radiation (Lyman-Werner band) destructs H_2 molecules, which is the main coolant below 10^4 K in low metallicity gas (Stecher & Williams 1967; Haiman, Rees, & Loeb 1997; Kitayama et al. 2001). Then, the formation of low mass objects with the virial temperature less than 10^4 K is suppressed. Moreover, no star is expected to form in ionized gas. Hence, to form star clusters, the gas cloud should be self-shielded from UV background radiation (Tajiri & Umemura 1998). To treat the self-shielding, we should solve the radiative transfer properly. Kitayama et al. (2001) explored the formation of dwarf galaxies within UV radiation fields, using spherical symmetric hydrodynamics coupled with the radiative transfer. With the radiation hydrodynamic (RHD) simulations, they showed that dwarf galaxies can form even after the reionization, if the self-shielding effectively works. Susa & Umemura (2004) also studied this issue by three-dimensional RHD simulations including formation of stars and the stellar dynamics. In their simulations, they showed that a dwarf galaxy with the stellar mass of $\approx 10^6 M_\odot$ is able to form even in UV radiation. The half-mass radius of the stellar system is ~ 100 pc, which is corresponding to the sizes of dSphs, but greater by about one-order magnitude

than the observed GC size. Hence, a further mechanism is required to produce much more compact star clusters in UV radiation.

In this paper, we explore a possibility that a superpersonally contracting cloud produces a compact star cluster in UV radiation. A gas cloud with its infall velocity exceeding the sound speed of ionized gas ($T \simeq 10^4\text{K}$) can keep contracting, even if the gas cloud is fully ionized. The contracting cloud is eventually shielded from both ionizing photons and H_2 dissociating photons, and then the cloud can cool via H_2 cooling, generating a star cluster. The star cluster formed through such a process becomes very compact due to strong energy dissipation.

This paper is organized as follows. In §2, the simulation code and numerical procedure are described. The results of simulations are presented in §3, and it is shown that the evolution of subgalactic objects are typically separated into three branches. The comparison with the observations of GCs, dSphs, and UCDs is given in §4. The specific frequencies of GCs, required UV intensity, tidal effects by host galaxy, and internal feedbacks are discussed in §5. §6 is devoted to the conclusions. Throughout this paper, we assume a Λ -CDM cosmology with the matter density $\Omega_M = 0.3$, the cosmological constant $\Omega_\Lambda = 0.7$, the Hubble constant $h = 0.7$, and the baryon density $\Omega_B = 0.05$.

2 SIMULATIONS

2.1 Numerical Scheme

We use a radiation-hydrodynamic scheme developed by Kitayama et al. (2001), to solve hydrodynamics coupled with radiative transfer. This scheme is based on the second-order Lagrangian finite-difference method in spherical symmetry. In this scheme, we treat self-consistently gravitational force of dark matter and baryon, hydrodynamics, non-equilibrium chemistry of primordial gas including H_2 , and the radiative transfer of ionizing photons. For self-shielding by H_2 against photo-dissociating photons, we employ the self-shielding function introduced by Draine & Bertoldi (1996). [See also Kitayama et al. (2001) for the details of scheme.] Initially, the number of shells is $N_b = 600$ for gas component and $N_d=10000$ for DM component. Shocks are treated with artificial viscosity. In order to investigate whether the results are sensitive to the treatment of artificial viscosity, we perform the simulations with stronger artificial viscosity (10 times as strong as the fiducial one) or weaker artificial viscosity (0.1 times as weak as the fiducial one). As a result, we find that the changes of results are only a few percent. Thus, we conclude that the present results are not sensitive to the treatment of artificial viscosity.

We also consider the formation of stars from cooled gas component and pursue the relaxation process of formed stars. We take the following conditions as the star formation criteria:

$$T_g < 2000\text{K}, \quad (1)$$

$$v_r < 0, \quad (2)$$

$$\frac{d\rho_g}{dt} > 0, \quad (3)$$

$$\frac{dT_g}{dt} < 0. \quad (4)$$

Here T_g , v_r , and ρ_g are the temperature, the infall velocity, and the density of gas shell. Ionized gas cannot cool below 10^4K , if satisfying the condition (3). Hence, the gas must be shielded against UV radiation to satisfy the condition (1). In that sense, the condition (1) is a most important criterion. However, the threshold temperature 2000K is not so crucial. When we changed this threshold temperature from 1000K to 5000K , we found no significant difference in the main results. We assume that if a gas shell satisfies all of the above conditions, the gas shell becomes a stellar shell immediately, since the timescale of star formation is basically the free-fall time in a high density region, which is considerably shorter than the dynamical timescale of the whole cloud.

The basic equation for the stellar dynamics is given by

$$\frac{d^2 r_s}{dt^2} = -\frac{GM_{\text{tot}}(< r_s)}{r_s^2}, \quad (5)$$

where r_s and $M_{\text{tot}}(< r_s)$ are the radius of stellar shell and the total mass (including baryon and DM components) inside r_s , respectively. For stellar shells, we allow them to cross each other. We also calculate the mass weighted velocity dispersion, which is represented by

$$\sigma_*^2 = \frac{\sum_n^{N_*} dm_{*,n} v_{*,n}^2}{M_{*,\text{tot}}}, \quad (6)$$

where N_* , $dm_{*,n}$, $v_{*,n}$ and $M_{*,\text{tot}}$ are the number of stellar shells, mass of n -th stellar shell, infall velocity of n -th shell and the total stellar mass, respectively.

2.2 Setup

The initial density distribution of a cloud consisting of gas and DM is the same as that in Kitayama et al. (2001). We calculate the evolution of the cloud from its linear overdensity stage. We concentrate on low-mass clouds with the initial baryonic mass of $10^5 M_\odot \lesssim M_{b,\text{in}} \lesssim 10^8 M_\odot$ collapsing at high redshifts $3 \lesssim z_c \lesssim 20$. Since we define z_c as the epoch at which a cloud as a whole collapses, the collapse redshift of the central high-density regions z_{c0} is earlier than z_c . These two redshifts are related by $1 + z_{c0} = 2.7(1 + z_c)$. When $z \leq z_{\text{UV}}$, the cloud is exposed to external UV radiation. Here, we assume the constant UV intensity specified by I_{21} , where I_{21} is the intensity at the Lyman limit frequency of hydrogen ν_L in units of $10^{-21} \text{erg cm}^{-2} \text{s}^{-1} \text{Hz}^{-1} \text{str}^{-1}$.

The cosmic reionization epoch is inferred to be $z_r \approx 11$ (Page et al. 2007; Komatsu et al. 2009). The reionization of intergalactic matter can start at earlier epochs in an inhomogeneous fashion (Nakamoto, Umemura & Susa 2001; Ciardi et al. 2001). Although the ionization sources are still uncertain, the reionization by Pop III stars has been considered as one of plausible possibilities (Gnedin 2000; Ciardi et al. 2001; Cen 2003; Sokasian et al. 2004). Here, we assume Pop III-type ionization sources. Previous studies have shown that Pop III stars are as massive as $\sim 100 M_\odot$ (e.g., Abel, Bryan & Norman 2000; Bromm, Coppi & Larson 2002; Nakamura & Umemura 2001; Yoshida et al. 2006). Then, the blackbody radiation with effective temperature of $T_{\text{eff}} \simeq 10^5 \text{K}$ is emitted from a Pop III star. The number of ionizing photons emitted per second is $\dot{N} \sim 10^{50} \text{s}^{-1}$ (Schaerer 2002). Since a Pop III

object is as massive as $10^6 M_\odot$ (e.g., Omukai & Nishi 1999; Yoshida et al. 2003), almost all ionizing photons emitted from a Pop III star can escape from the Pop III object (Kitayama et al. 2004). Qualitatively, the virial radius of the Pop III object is given by

$$R_{\text{vir}} = 1.60 \times 10^2 \left(\frac{M_f}{10^6 M_\odot} \right)^{1/3} \left(\frac{20}{1+z_c} \right) \text{pc}, \quad (7)$$

where M_f is the total mass of the Pop III object and z_c is its collapse redshift. On the other hand, the Strömngren sphere, which is estimated for the cosmic mean density, is extended to the radius

$$R_s = 5.45 \times 10^3 \left(\frac{\dot{N}}{10^{50}} \right)^{1/3} \left(\frac{20}{1+z} \right)^2 \text{pc}. \quad (8)$$

If the radiation flux from a Pop III star is translated into an averaged intensity I_ν , we have

$$I_\nu = B_\nu(T_{\text{eff}}) \left(\frac{R_*}{r} \right)^2. \quad (9)$$

Under the assumption that one Pop III star is born in a halo, the UV intensity is evaluated to be from $I_{21} \sim 10^3$ at the virial radius of PopIII halo to $I_{21} \sim 10^{-3}$ at the Strömngren radius. Hence, we investigate the range of $10^{-3} \leq I_{21} \leq 10^3$. As for UV irradiation epoch, we investigate three cases as $z_{\text{UV}}=15, 20$, or 25 .

3 RESULTS OF SIMULATIONS

3.1 Hydrodynamics and star formation

If a cloud is not irradiated by UV radiation or self-shielded from a UV background, it cools down to several 100K by H_2 cooling. Then, a cloud more massive than the Jeans mass of 100K, $M_J(100\text{K}) \sim 10^5 M_\odot$, can collapse to form stars. When a cloud is photoionized, the gas temperature is raised up to $\approx 10^4\text{K}$, and then the Jeans mass increases to $M_J(10^4\text{K}) \sim 10^8 M_\odot$. If the cloud mass is below $M_J(10^4\text{K})$, the ionized gas cannot be confined to a DM halo, but evaporated. Nevertheless, if the infall velocity exceeds the sound speed of 10^4K , the ionized gas can collapse even when the total mass is below $M_J(10^4\text{K})$. Thus, the hydrodynamic evolution of gas cloud and subsequent star formation are sensitively dependent on the total mass of cloud, the strength of self-shielding, and the infall velocity. In the following, we show the typical numerical results, which are basically categorized into three types of evolutionary branches.

3.1.1 Prompt star formation (strong evaporation)

This is the case of the cloud mass between $M_J(100\text{K})$ and $M_J(10^4\text{K})$. When external UV radiation irradiates the cloud, the inner regions at $r < R_{\text{shield}}$ are promptly self-shielded to form stars. But, the outer envelope of cloud is photoionized and evaporated due to the enhanced thermal pressure, because $M < M_J(10^4\text{K})$. The schematic view is shown in Fig. 1 (top panel). The cloud evolution is shown in Fig. 2, where the mass shell evolution is shown around the self-shielding radius R_{shield} . After the cloud is irradiated by external UV, a shell inside R_{shield} can collapse, because the self-shielded mass is higher than $M_J(100\text{K})$. Eventually, the

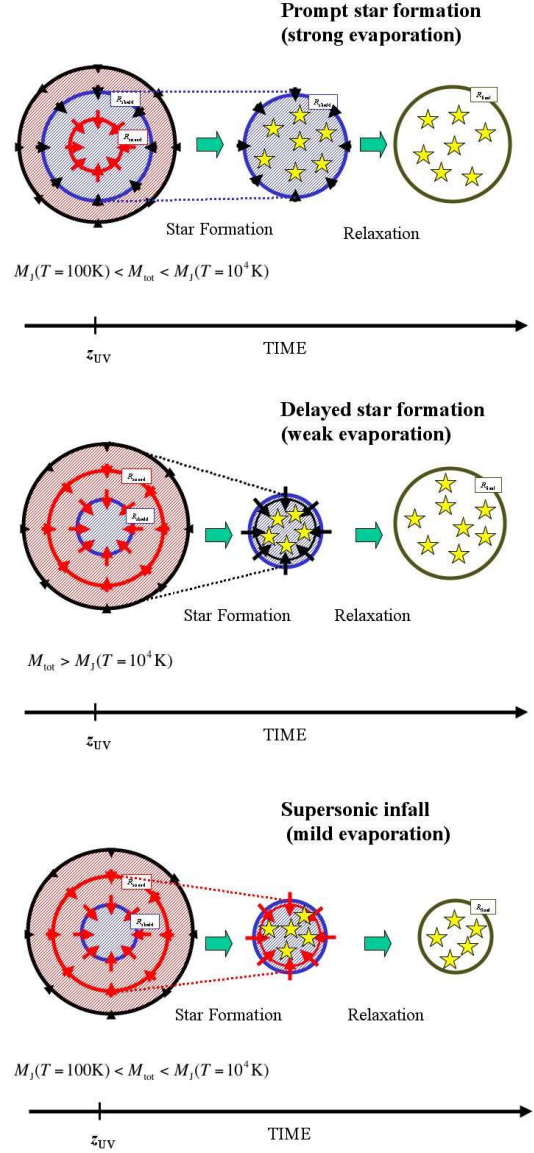


Figure 1. Schematic views for the *prompt star formation* case (top panel), the *delayed star formation* case (middle panel), and the *supersonic infall* case (bottom panel). In each panel, arrows indicate infall velocity vectors. Blue circles indicate the self-shielding radii R_{shield} , inside which the gas is impervious to external UV radiation and therefore can cool by H_2 cooling to form stars. Red circles indicate the sonic point R_{sonic} , where the infall velocity corresponds to the sound speed of 10^4K .

shell cools down, forming stars promptly. In this case, the star formation criteria is satisfied from inside out to R_{shield} . The duration of star formation is roughly 10-100Myr. The duration is longer for higher mass clouds, since a larger part of massive clouds can be shielded. On the other hand, the regions outside R_{shield} are ionized and photoheated. Then, shells there evaporate shortly.

As a result, the mass-to-light ratios are expected to be higher owing to the mass loss by the photoevaporation. Such behaviors can be basically understood as the formation mechanism of dwarf galaxies in a UV back-

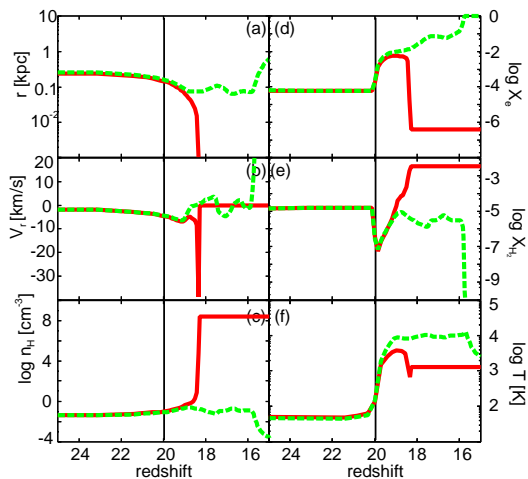


Figure 2. Cloud evolution in the case of *prompt star formation*. The physical quantities around the self-shielding radius are shown as a function of redshift, with (a) radii, (b) infall velocity, (c) hydrogen number density, (d) electron fraction, (e) H_2 fraction, and (f) gas temperature of the cloud. The parameters here are $z_{UV} = 20$, $M_{b,in} = 10^6 M_\odot$, $z_c = 7$, and $I_{21} = 1$. In each panel, a thick solid line shows the shell that finally collapses, while a thick dashed line shows the shell that finally evaporates. A thin vertical solid line indicates the epoch of UV irradiation, z_{UV} .

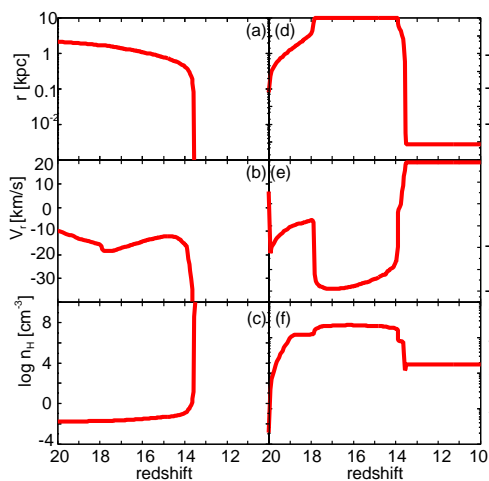


Figure 3. Cloud evolution in the case of *delayed star formation*. The physical quantities same as those in Fig. 2 are shown. The parameters here are $z_{UV} = 20$, $M_{b,in} = 10^8 M_\odot$, $z_c = 7$, and $I_{21} = 100$. The time evolution of the outermost shell that finally collapses is shown.

ground that is previously studied in detail by several authors (e.g., Kitayama et al. 2001; Susa & Umemura 2004; Ricotti, Gnedin & Shull 2008).

3.1.2 Delayed star formation (weak evaporation)

This is the case of cloud mass slightly higher than $M_J(10^4K)$. When UV intensity is very weak, the almost all regions of cloud are self-shielded and collapse in a similar way to the UV-free case. However, if external UV is relatively strong, the bulk of cloud is photoionized. No star forms in the ionized regions, since no H_2 cooling works there.

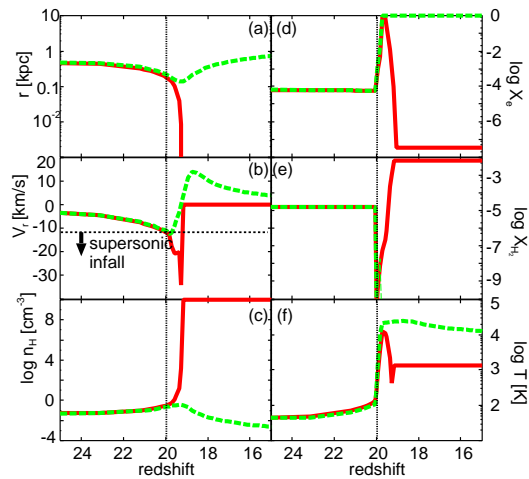


Figure 4. Cloud evolution in the case of *supersonic infall*. Same as Fig. 2, except for $M_{b,in} = 10^7 M_\odot$ and $I_{21} = 100$. In panel (b), the sound speed of 10^4K is shown by the horizontal dotted line. The time evolution of shells around the sonic point is shown.

Nonetheless, most of ionized regions do not evaporate but collapse, because the cloud is more massive than $M_J(10^4K)$ and therefore the self-gravity overwhelms the pressure of the ionized gas. As a result, in the course of cloud contraction, the ionized regions are self-shielded due to the increase of density. Then, stars form there in a delayed fashion. In this case, the star formation can continue for $> 100\text{Myr}$ because of the delayed self-shielding. The schematic view is shown in Fig. 1 (middle panel). The cloud evolution in a strong UV background is shown in Fig. 3, where the outermost shell that finally collapses is shown. The shell is ionized after $z_{UV} = 20$, but it collapses and is self-shielded around $z = 14$, forming a cooled shell. As a result of such delayed self-shielding, a formed star cluster can become more compact than a star cluster formed in no UV background, and therefore the stellar velocity dispersion of cluster is increased. It is noted that the effect of delayed star formation becomes conspicuous for the mass slightly above $M_J(10^4K)$, since a much higher mass cloud is impervious to photoionization except for surface thin layer.

3.1.3 Supersonic infall (mild evaporation)

This is a novel branch that is found in the present simulations. The cloud mass is between $M_J(100K)$ and $M_J(10^4K)$, similar to the case of prompt star formation, but the infall velocity of the cloud can exceed the sound speed of 10^4K owing to radiative cooling as well as a potential of DM halo. When the cloud is exposed to strong UV radiation, ionizing photons permeate the cloud deeply, and a large part of cloud is photoionized. However, shells collapsing with supersonic infall velocities cannot be stopped by photoheating. Therefore, they keep contracting, regardless of photoionization. Such shells are eventually self-shielded, when the density increases sufficiently due to the contraction, and then forms a compact star cluster. The schematic view of the supersonic infall case is shown in Fig. 1 (bottom panel). The evolution of shells around the sonic point is shown in Fig. 4. A dotted line shows an evaporating shell, while a solid line shows

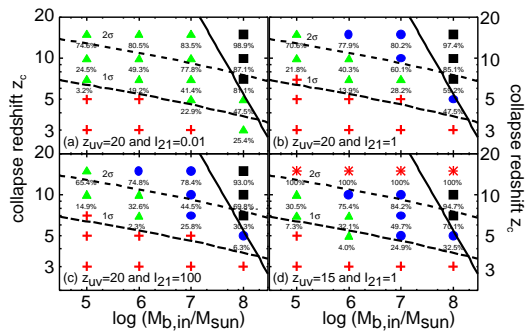


Figure 5. Dependence of cloud evolution on the cloud mass, collapse epoch, UV intensity, and UV irradiation epoch. The collapse redshift z_c and the type of evolution are shown against the initial baryonic mass of cloud, $M_{b,in}$. Panels (a), (b) and (c) show the results with $z_{UV} = 20$, but for different UV intensity as $I_{21} = 0.01$, $I_{21} = 1$, and $I_{21} = 100$, respectively. Panel (d) is the result of $z_{UV} = 15$ and $I_{21} = 1$. Triangles, squares, and circles indicate the cases of *prompt star formation*, *delayed star formation*, and *supersonic infall*, respectively. Pluses represent complete evaporation, and asterisks correspond to evolution in no UV. The percentages attached to the symbols represent the fraction of the final stellar mass M_* to the initial baryonic mass, $M_*/M_{b,in}$. In each panel, a long-dashed and a short-dashed line correspond to 1σ and 2σ CDM fluctuations. A solid line represents the Jeans mass of ionized gas $M_J(10^4\text{K})$.

a collapsing shell with supersonic infall velocity. It is clear that the supersonic infall shell is photoionized once (panel b), and eventually self-shielded from both ionizing photons (panel d) and H_2 -dissociating photons (panel e), and cools below 10^4K (panel f) by H_2 cooling. Hence, the gas inside the sonic point R_{sonic} results in a compact star cluster.

As a result, the strong contraction before star formation enhances the stellar velocity dispersion to a large degree. As a matter of importance, in this *supersonic infall* case, the duration of star formation becomes less than 10Myr, in contrast to the other two cases. This means almost coeval star formation, which is consistent with the fact that GCs commonly have a single stellar population. The *supersonic infall* branch appears if the sonic point is larger than the self-shielding radius.

3.2 Parameter Dependence

The dependence of cloud evolution on the mass, collapse epoch, UV intensity, and UV irradiation epoch are summarized in Fig. 5. In each panel, the resultant types of evolution are shown in the diagram of the collapse redshift against the initial baryonic mass of cloud. Also, 1σ and 2σ CDM density fluctuation spectra are shown. The UV intensity is changed with $I_{21} = 10^{-2}$, 1 or 10^2 . In the panels (a), (b) and (c), the UV irradiation epoch is assumed to be $z_{UV} = 20$, while $z_{UV} = 15$ in the panel (d). In the simulations with $z_{UV} = 15$, the objects collapsed before $z = 15$ correspond to the UV-free case. Interestingly, the boundary between the complete evaporation and star cluster formation roughly corresponds to 1σ CDM fluctuation.

In each panel, a thin solid line indicates the Jeans mass of ionized gas $M_J(10^4\text{K})$, which is given by

$$M_J(10^4\text{K}) = 1.1 \times 10^9 M_\odot (1+z_c)^{-3/2} \left(\frac{\Omega_b}{0.05} \right) \left(\frac{\Omega_M}{0.3} \right)^{-1}. \quad (10)$$

Above this line, the cloud evolution results in the *delayed star formation* as seen in Fig. 5. Below the Jeans mass $M_J(10^4\text{K})$, clouds with more massive and higher collapse epochs lead to the star cluster formation by the *supersonic infall*. This tendency can be understood by following two reasons: (i) The self-shielding radius is weakly dependent on the cloud mass ($R_{\text{shield}} \propto M^{2/3}$) shown by Tajiri & Umemura (1998), while the radius where the infall velocity exceeding the sound speed is roughly proportional to the cloud mass. Hence, a higher mass cloud has larger ionized, supersonic regions. (ii) The fraction of supersonic infall regions becomes larger according as the cloud contracts. Thus, earlier collapsing clouds tends to form most stars through supersonic infall.

In $z_{UV} = 15$ simulations, the trend is the same as the simulations with $z_{UV} = 20$, as long as the collapse epoch is later than $z_{UV} = 15$. On the other hand, in the case of weak UV with $I_{21} = 10^{-2}$ (panel a), the *supersonic infall* case does not appear, because the self-shielding radius is always larger than the sonic point.

3.3 Stellar Dynamics

Here, we pursue the subsequent stellar dynamics of star clusters formed through three mechanisms shown above. In Fig. 6, the time sequence of mass distributions is shown for *prompt star formation*, *delayed star formation*, and *supersonic infall* cases. Obviously, the mass distribution of a star cluster formed through the *supersonic infall* is different from the other two cases. In the *supersonic infall* case, the stellar component is predominant in the inner several 10pc regions. On the other hand, in the other two cases, the system is dominated by the DM component in almost all regions. These results are understood as follows: In the *supersonic infall* case, the star formation is delayed by the external UV radiation, until the cloud contraction eventually causes the self-shielding. Then, the strong energy dissipation occurs in a compact region, leading to the formation of a dense star cluster. As a result, a compact star-dominant system forms. On the other hand, in the *prompt star formation* case, stars are born at earlier dynamical phase of initially self-shielded regions. Consequently, the energy dissipation is not so strong and therefore a more diffuse star cluster forms. In the *delayed star formation* case, the cloud is self-shielded after it contracts to some degree. Hence, the dark matter contribution becomes smaller compared to the *prompt star formation* case. But, it does not grow into a totally star-dominant system, since the cloud is self-shielded before it becomes baryon-dominated. Thus, we conclude that the *supersonic infall* is only the branch that produces star-dominant compact clusters.

4 COMPARISON WITH OBSERVATIONS

4.1 Mass-to-light ratios and half-mass radii

As shown in §3, the final mass-to-light ratios depend on the formation processes. Here, we derive the mass-to-light

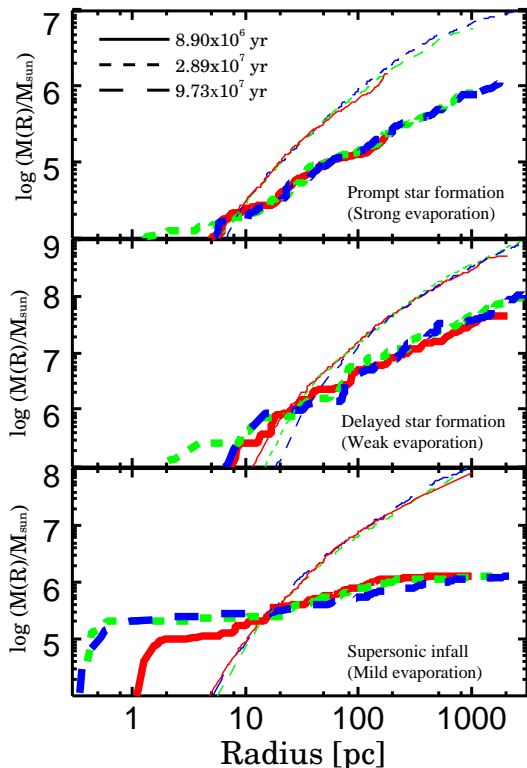


Figure 6. Mass distributions for typical three cases: *prompt star formation* case (top panel), *delayed star formation* case (middle panel), and *supersonic infall* case (bottom panel). In each panel, time variations of mass distributions are shown by $M(R)$ in units of the solar mass, where $M(R)$ is the cumulative mass in the regions of $r \leq R$. Thick lines show stellar components, while thin lines do DM components. Solid, short-dashed, and long-dashed lines are respectively corresponding to the distributions at 8.9×10^6 yr, 2.89×10^7 yr and 9.73×10^7 yr after z_{UV} .

ratios of simulated objects. In this section, we use simulation results with $z_{UV} = 20$, $I_{21} = 10^{-2}, 1$, or 10^2 , $M_{b,in} = 10^5 M_\odot - 10^8 M_\odot$, and $z_c = 5$ or 7 , which corresponds to the central collapse redshift of $z_{c0} \approx 15.2$ or 20.6 , respectively. For each simulated object, the dynamical mass is evaluated by the total mass ($M_{dyn} = M_* + M_{DM}$) inside the half-mass radius of the stellar component. As for stellar components, we assume $M_*/L_V = 2$, where M_* is the total stellar mass and L_V is the V-band luminosity (Pryor & Meylan 1993). This is a typical value when stars produced by initial starbursts evolve for 10 Gyr. In Fig. 7, the resultant mass-to-light ratios M_{dyn}/L_V of simulated objects are shown as a function of absolute V-band magnitude M_V , and they are compared to the observations of globular clusters (GCs), dwarf spheroidals (dSphs), and ultra-compact dwarfs (UCDs).

As seen clearly, the models of *prompt star formation*, *delayed star formation*, and *supersonic infall* are distinctively separated in this diagram. In particular, the model of *supersonic infall* matches fairly well with bright GCs. It is worth noting that even if we change M_*/L_V by a factor of 2, it does not alter basic results significantly. The models of *prompt star formation* and *delayed star formation* seem to match dSphs and UCDs, respectively in this diagram. However, these two models can be affected by internal feedbacks.

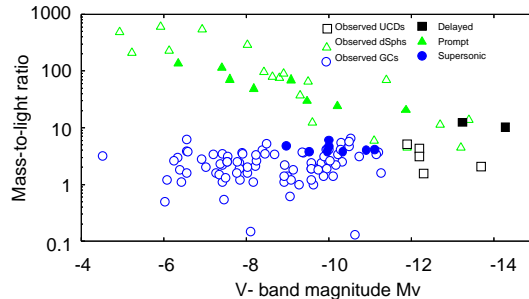


Figure 7. Mass-to-light ratios as a function of absolute V-band magnitude M_V . Large filled symbols are simulations, while small open symbols are observations. Filled triangles, filled squares, and filled circles indicate the objects formed through *prompt star formation*, *delayed star formation*, and *supersonic infall*, respectively. On the other hand, open triangles, open squares, and open circles indicate observed dwarf spheroidals (dSphs), ultra-compact dwarfs (UCDs), globular clusters (GCs), respectively. The observational data of GCs are taken from the data of Milky Way GCs (Pryor & Meylan 1993), M31 GCs (Fischer et al. 1993; Dubath et al. 1996; Djorgovski et al. 1997), LMC GCs (Dubath & Grillmair 1997; Fischer et al. 1993), SMC GCs (Dubath et al. 1992), and NGC5218 GCs (Martini & Ho 2004). The data of dSphs are taken from Mateo (1998), Matin et al. (2006), Simon & Geha (2007), McConnachie & Irwin (2006), and Majewski et al. (2007). The UCD data are taken from Drinkwater et al. (2003).

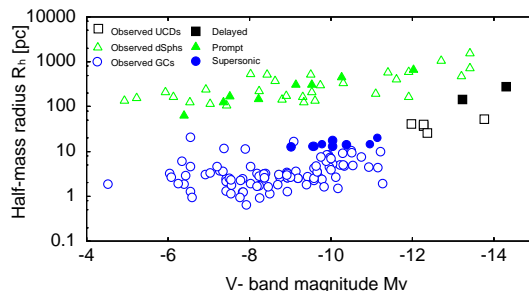


Figure 8. Half-mass radii R_h as a function of absolute V-band magnitude M_V . The symbols are the same sense as Fig. 7.

The effects by the internal feedback are discussed meticulously in the next section. Anyhow, if the final M_*/L_V for stellar components is in the range of $1 \lesssim M_*/L_V \lesssim 4$, three models are distinctive in this diagram. The mass loss by internal feedbacks in *prompt star formation* and *delayed star formation* would result in an up-shift in Fig. 7, leading to a further deviation from GCs.

Also, in Fig. 8, the resultant half-mass radii R_h of simulated objects are shown as a function of absolute V-band magnitude M_V , and compared the observations. Again, the model of *supersonic infall* is well concordant with observed bright GCs, whereas the other two models are not. Here, a remarkable property for the *supersonic infall* model is that the half-mass radius is almost independent of the mass. This is due to the fact that a higher mass cloud has larger ionized, supersonic region, and eventually the energy dissipation occurs more strongly. It is worth noting that half-mass radii in *prompt star formation* case are about tens times larger than those in *supersonic infall* case for the same luminosity

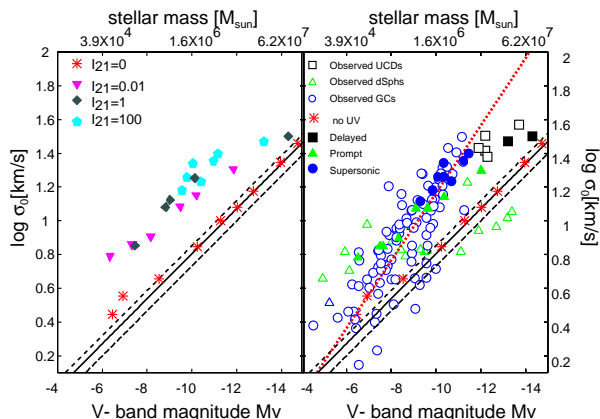


Figure 9. Velocity dispersions σ_* as a function of absolute V-band magnitude M_V . In the left panel, the dependence on UV intensity is shown. Asterisks, reverse triangles, diamonds, and pentagons represent the results for $I_{21} = 0$, $I_{21} = 0.01$, $I_{21} = 1$, and $I_{21} = 100$, respectively. The virial relation expected in the UV-free case are also shown by a long-dashed, a solid, and a short-dashed line, respectively for the collapse epoch of $z_c = 5, 7$, and 10. In the right panel, the simulation results are compared with the observational data, where the meanings of symbols are the same as Fig. 8. The best fit relation for the observed GCs is shown by a dotted line.

range. These results imply that UV background radiation works significantly to determine the properties of subgalactic objects. The final mass-to-light ratios and half-mass radii are both responsible for the velocity dispersions of objects.

4.2 Velocity dispersions

In Fig. 9, the stellar velocity dispersion σ_* of simulated objects are shown as a function of absolute V-band magnitude M_V . Here, we also show the results with $I_{21} = 0$ (UV-free case), assuming $M_*/L_V = 2$. In the left panel, the dependence on UV background intensity is shown for $I_{21} = 0$, $I_{21} = 0.01$, $I_{21} = 1$, and $I_{21} = 100$. Also, the relation ($L \propto \sigma_*^3$) predicted from the virial theorem in the UV-free case is shown for the collapse redshifts of $z_c = 5, 7$, and 10. The objects without UV effects well follow this prediction. In the presence of the UV background radiation, systematically larger velocity dispersions are predicted for a given V-band magnitude.

In the right panel, the simulation results are compared with observational data. The objects formed through *supersonic infall* are distributed near the best fit relation for the observed GCs shown by a dotted line. It should be noted that only the *supersonic infall* case can account for GCs with high velocity dispersions $\gtrsim 10 \text{ km s}^{-1}$. For the *supersonic infall* case, higher mass clouds result in the stronger energy dissipation. Consequently, the relation between σ_* and M_V becomes steeper than that the UV-free case ($\sigma_* \propto L^{1/3}$). The correlation for the *supersonic infall* case is roughly given by $\sigma_* \propto L^{1/2}$, which is consistent with the observed GCs (e.g., McLaughlin & van der Marel 2005). Since velocity dispersions are estimated as $\sigma_* \propto \sqrt{GM/R}$, this relation implies that the radii of objects is almost regardless of the mass. This is consistent with the resultant half-mass radii R_h shown in Fig. 8.

The velocity dispersions for the *delayed star formation* case are systematically larger than the prediction by the simple virial theorem, since the energy dissipation is stronger than that in the UV-free case. In this diagram, the velocity dispersions for *supersonic infalling* case and *prompt star formation* case are degenerated at $-8 \geq M_V \geq -10$. But, the origin is different, since the distributions in mass-to-light ratios and half-mass radii are well separated as shown above. Since the outer regions of cloud evaporates in the *prompt star formation* case, the velocity dispersion is determined basically by the DM component.

In Figs. 7, 8, and 9, the *supersonic infall* does not reproduce faint GCs in the range of $-6 > M_V > -9$. If we subdivide the parameter space near the low-mass boundary between the models of *supersonic infall* and *prompt star formation*, compact star clusters like faint GCs possibly appear. Another possibility is the mass loss through tidal stripping by a host galaxy, which results in low-mass GCs.

5 DISCUSSION

5.1 Specific frequencies

It is known that early-type galaxies have higher specific frequency of GCs than late-type galaxies (Harris 1991). Moreover, the specific frequency depends on the luminosity of host galaxy (Forbes 2005; Bekki et al. 2006). The specific frequency S_N is defined as the GC population normalized to $M_{V,\text{host}} = 15$ as

$$S_N \equiv N_t \times 10^{0.4(M_{V,\text{host}} + 15)}, \quad (11)$$

where N_t is the total number of GCs in a host galaxy and $M_{V,\text{host}}$ is the V-band magnitude of host galaxy. This tendency could be qualitatively understood by combining the present results with the galaxy formation theory in UV background radiation, which is studied by Susa & Umemura (2000). Susa & Umemura (2000) have shown that early-type galaxies form more preferentially at high- σ peak regions of CDM fluctuations, since the self-shielding works effectively to allow the high efficiency of star formation and therefore the galaxy formation proceeds in a dissipationless fashion. The present simulations have shown that GCs can also form preferentially from high- σ fluctuations ($> 2\sigma$) as shown in Fig. 5. Therefore, it is expected that the number of GCs around an early-type galaxy tends to be larger than that in a late-type galaxy.

Moore et al. (2006) have explored the spatial distribution of subhalos in host galaxies, by high-resolution N -body simulations. They have found that the spatial distributions of subhaloes originating in high- σ peaks ($> 2.5\sigma$) are similar to those of old metal-poor GCs in the Milky way galaxy. Thus, it is likely that objects by the *supersonic infall* can correspond to the metal-poor GCs in host galaxies.

Saitoh et al. (2006) have carried out hydrodynamic simulations on the galaxy formation with high spatial resolution. It is found that numerous clumps of globular cluster mass scale form in a host galaxy. The specific frequency S_N can be roughly estimated to be the $S_N \sim 20$, assuming the mass-to-light ratio of $M/L_V = 5$. On the other hand, the specific frequency in spiral galaxies is observed to be $S_N \simeq 1$ (Harris 1991). This implies that not all the small

mass clumps do not evolve into GCs. Here, we have shown that only the *supersonic infall* branch can lead to the formation of GCs. Hence, a portion of small mass clumps evolve into GCs. To make quantitative argument, it is necessary to perform high resolution simulations on the galaxy formation including the radiative transfer effect of UV background radiation. This would be a future challenge.

5.2 Sites of GC formation

As shown in Fig. 5, the *supersonic infall* case does not appear in the simulations with $I_{21} \leq 0.01$. If there is no or very weak UV radiation fields, only low density star clusters form (top panel in Fig. 6). To form compact star clusters like GCs, strong UV radiation, roughly $I_{21} > 1$ is required. Massive Population III stars are one possibility to produce strong UV intensity in high redshift epochs. But, the strong UV radiation is relatively localized in HII region around a Population III halo (Susa & Umemura 2006; Hasegawa, Umemura & Susa 2009). Another possibility is black hole accretion that could be a more powerful source (Ricotti & Ostriker 2004; Susa & Kitayama 2000). Susa & Kitayama (2000) simply estimated the UV intensity around AGN of $10^{44} \text{erg s}^{-1}$ as

$$I_{\nu_L} \sim 1 \times \left(\frac{100 \text{kpc}}{R_g} \right)^2 \times 10^{-21} \text{erg s}^{-1} \text{cm}^{-2} \text{str}^{-1}, \quad (12)$$

where R_g is the distance from the black hole. That is to say, $I_{21} \sim 1$ is achieved at 100kpc around an AGN. This can allow the GC formation in a fairly wide area around the host galaxy.

5.3 Tidal stripping

It is expected that the evolution of star clusters can be affected by the tidal force by its host galaxy (i.e. Mashchenko & Sills 2005). The importance of the tidal interaction is estimated as follows. The balance between the self-gravity and the tidal force is given by

$$\frac{Gm^2(< r_t)}{r_t^2} \approx \frac{2GM_{\text{host}}m(< r_t)r_t}{R_c^3}, \quad (13)$$

where r_t , $m(< r_t)$, M_{host} and R_c are the tidal radius, the cluster mass inside r_t , the host galaxy mass and the position of star cluster from the centre of host galaxy, respectively. GCs are likely to form in small proto-galaxies in the early universe (e.g., Bromm & Clarke 2002; Mashchenko & Sills 2005). Hence, we assume that $M_{\text{host}} = 10^9 M_\odot$ and $R_c = 0.3\text{--}1 \text{kpc}$. If we use the distributions obtained by the present simulations, the tidal radii r_t are evaluated as 10pc - 50pc for the *supersonic infall* case (bottom panel in Fig. 6). This value is larger than the half-mass radii of GCs shown in Fig. 8. This implies that the estimation of mass-to-light ratios or velocity dispersions for the *supersonic infall* case is not affected, even if the outer diffuse DM halo is stripped away by the tidal force. Unfortunately, it is difficult to argue precisely the evolution of star clusters in the tidal fields by one-dimensional simulations. Hence, we need to simulate the three-dimensional dynamical evolution by means of N -body method. We are going to present such N -body simulations in a forthcoming paper.

5.4 Internal feedbacks

Our calculations do not include the internal feedback, i.e., UV radiation from internal massive stars and supernova (SN) explosions, which becomes important in the case of successive star formation. As mentioned above, the duration of star formation in *supersonic infall* case is typically several Myrs. The binding energy of a star cluster produced by *supersonic infall* is in the order of 10^{51}erg , which corresponds to the typical SN energy. Hence, only one massive SN can sweep away the interstellar gas. Therefore, the *supersonic infall* results in a single stellar population, which is consistent with observed GCs. It is also important to mention that such a short duration of star formation may also be responsible for the chemical homogeneity observed in individual GCs.

On the other hand, much larger stellar metallicity dispersions found in dwarf galaxies may be due to successive star formation. In the cases of *prompt star formation* and *delayed star formation*, the duration of star formation is 10 - 1000Myr, and the binding energy roughly ranges from 10^{51}erg to 10^{54}erg . The importance of internal feedbacks is likely to depend on the mass scale. In the case of $M_{\text{b,in}} < 10^7 M_\odot$, the duration of star formation is shorter (several 10Myr) as shown in §3.1, since the star formation is quickly quenched by the external UV radiation. In addition, SN explosions as well as stellar UV radiation would significantly suppress subsequent star formation (Kitayama et al. 2004; Kitayama & Yoshida 2005). Interestingly, a recently discovered "faint" dSph Ursa Major I shows a single old stellar population (Okamoto et al. 2008). The low-luminous *prompt star formation* model might correspond to such "faint" dSphs. On the other hand, in the case of $M_{\text{b,in}} > 10^7 M_\odot$, successive star formation is possible even if the cloud is irradiated by the external UV radiation. Moreover, repeated SN explosions, which might trigger the star formation, are possible owing to the fact that the binding energy is larger than $\sim 10^{51} \text{erg}$. Hence, in this case, the present simulations should not be directly compared with observations. The final states would be determined by internal feedbacks as shown in Dong, Lin & Murray (2003). They have studied the effect of the internal feedbacks by UV and SN explosions of formed stars as well as the external UV feedback on the formation of dSphs, by spherical symmetric simulations. They have shown that the star formation in low-mass dSphs is severely suppressed by the external UV radiation, whereas the star formation in high-mass dSphs is self-regulated by the internal feedback processes, and the final equilibria are determined solely by the internal feedback. Interestingly, their simulations have succeeded in reproducing multiple stellar population, which is observed in some dSphs in the Local Group (e.g., Grebel 1997; Ikuta & Arimoto 2002; Grebel & Gallagher 2004; Tolstoy et al. 2004).

This argument can be also applied in *delayed star formation* case. Although the final state is likely to be determined by the internal feedbacks, the external UV works to delay the onset of star formation. Owing to such an effect, the energy dissipation becomes slightly strong, which leads to the enhancement of velocity dispersion at a central region (middle panel of Fig. 6). Observed UCDs (Drinkwater et al. 2003) might be explained by this process (see Fig. 9).

While the important processes of internal feedbacks

has been studied by Dong, Lin & Murray (2003) in spherical symmetry, there are also three-dimensional effects. Susa & Umemura (2004) performed three-dimensional radiation hydrodynamic simulations with solving radiative transfer to investigate the shielding effect of local density peaks within a UV background. They have shown the local shielding allows the long duration of star formation even after the reionization. In addition, interstellar medium is compressed intricately by shocks produced by multiple SN explosions, and therefore the star formation would be triggered by such explosions (Mori, Ferrara & Madau 2002). Moreover, we mention that the dynamics of stars would be more complex, owing to three-dimensional effects (Aarseth, Lin & Papaloizou 1988; Murray & Lin 1996). These three-dimensional effects can play important roles for the star formation history and the dynamics of stars. Thus, we plan to carry out three-dimensional RHD simulations including the external radiation as well as the internal feedback to explore the star formation history comprehensively.

6 SUMMARY

We have carried out the radiation hydrodynamic simulations to explore the possibility that the formation of GCs is induced by external UV radiation fields. As a result, we have found that the *supersonic infall* enables a low-mass gas cloud to form a compact star cluster in the external UV radiation. A gas cloud with its infall velocity exceeding the sound speed can keep contracting, even if the gas cloud is fully ionized without the self-shielding from external UV radiation. The contracting cloud is shielded from a UV background when a compact cloud core forms, and cools by H₂ cooling. Consequently, a compact star cluster forms in a diffuse DM halo. We have also calculated the dynamical evolution of stars. It is found that resultant mass-to-light ratio, half-mass radius, and velocity dispersion of simulated star clusters match well with those of observed GCs. Therefore, the *supersonic infall* in a UV background is a promising mechanism to form GCs.

ACKNOWLEDGMENTS

We would like to thank N. Arimoto, H. Hirashita, D. N. C. Lin, T. Nakamoto, M. Ricotti, and K. Yoshikawa for valuable comments that considerably improved the manuscript. Numerical simulations have been performed with computational facilities at Centre for Computational Sciences in University of Tsukuba. This work was supported in part by the FIRST project based on Grants-in-Aid for Specially Promoted Research by MEXT (16002003), and Grant-in-Aid for Scientific Research (S) by JSPS (20224002). Also, it was supported in part by Grant-in-Aid for young Scientists (B) by MEXT (18740112, 21740139).

REFERENCES

- Aarseth, S. J., Lin, D. N. C., Papaloizou, J. C. B., 1988, ApJ, 324, 288
 Abel, T., Bryan, G. L., Norman, M. L., 2000, ApJ, 540, 39
 Ashman, K. M., Zepf, S., 1992, ApJ, 384, 50
 Ashman, K. M., Zepf, S., 2001, ApJ, 122, 1888
 Bekki, K., Yahagi, H., Forbes, D. A., 2006, ApJ, 645, L29
 Bromm, V., Clarke, C., 2002, ApJ, 566, L1
 Bromm, V., Coppi, P. S., Larson, R. B., 2002, ApJ, 564, 23
 Cen R., 2003, ApJ, 591, L5
 Ciardi B., Ferrara A., Marri S., Raimondo G., 2001, MNRAS, 324, 381
 Djorgovski, S. G., Gal, R. R., McCarthy, J. K., Cohen, J. G., de Carvalho, R. R., Meylan, G., Bendinelli, O., Parmeggiani, G. 1997, ApJ, 474, L19
 Dong, S., Lin, D. N. C., Murray, S. M., 2003, ApJ, 596, 930
 Draine, B. T., Bertoldi, F., 1996, ApJ, 468, 269
 Drinkwater, M. J., Gregg, M. D., Hilker, M., Bekki, K., Couch, W. J., Ferguson, H. C., Jones, J. B., Phillipps, S. 2003, Nature, 423, 519
 Dubath, P., Meylan, G., Mayor, M., 1992, ApJ, 400, 510
 Dubath, P., Reipurth, Bo., Mayor, M., 1996, A & A 308, 107
 Dubath, P., Grillmair, C. J., 1997, A & A 321, 379
 Fall, S. M., Rees, M. J. 1985, ApJ, 298, 18
 Fischer, P., Welch, D. L., Mateo, M., Cote, P., 1993, ApJ, 106, 1508
 Forbes, D. A., 2005, ApJ, 635, L137
 Gnedin N. Y., 2000, ApJ, 535, 530
 Grebel E. K., 1997, Reviews in Modern Astronomy, 10, 29
 Grebel E. K., Gallagher J. S., III, 2004, ApJ, 610, L89
 Haiman Z., Rees M. J., Loeb A., 1997, ApJ, 476, 458
 Harris, W. E. 1991, ARA & A, 29, 543
 Hasegan, M. et al. 2005, ApJ, 627, 203
 Hasegawa, K., Umemura, M., Susa, H., 2009, MNRAS, 395, 1280
 Ikuta, C., & Arimoto, N. 2002, A & A, 391, 55
 Kitayama, T., Susa, H., Umemura, M., Ikeuchi, S. 2001, MNRAS, 326, 1353
 Kitayama, T., Yoshida, N., Susa, H., Umemura, M. 2004, ApJ, 613, 645
 Kitayama, T., Yoshida, N., 2005, ApJ, 630, 675
 Komatsu, E. et al. 2009, ApJS, 180, 330
 Kravtsov, A. V., Gnedin, O. Y., 2005, ApJ, 623, 650
 Majewski, S. R., et al . 2007, ApJ, 670, L9
 Martini, P., Ho, L. C., 2004, ApJ, 610, 233
 Mashchenko, S., Sills, A. 2005, ApJ, 619, 258
 Mateo, M. L., 1998, ARA&A, 36, 435
 Matin, N. F., Ibata, R. A., Irwi, M. J., Chapman, S., Lewis, G. F., Ferguson, A. M. N., Tanvir, N., McConnachie, A. W., 2006, MNRAS, 371, 1983
 Mori, M., Ferrara, A., Madau, P., 2002, ApJ, 571, 40
 McConnachie, A. W., Irwin, M. J., 2006, MNRAS, 365, 1263
 McLaughlin, D. E., 1999, AJ, 117, 2398
 McLaughlin, D. E., van der Marel, R. P. 2005, ApJS, 161, 304
 Moore, B., Diemand, J., Madau, P., Zemp, M., & Staidel, J., 2006, MNRAS, 368, 563
 Murray, S. M., Lin, D. N. C., 1992, ApJ, 400, 265
 Murray, S. M., Lin, D. N. C., 1996, ApJ, 467, 728
 Nakamoto, T., Umemura, M., Susa, H., 2001, MNRAS, 321, 593
 Nakamura F., Umemura M., 2001, ApJ, 548, 19
 Okamoto, S., Arimoto, N., Yamasa, Y., Onodera, M., 2008, A&A, 487, 103

- Omukai, K., Nishi, R., 1999, *ApJ*, 518, 64
 Page, L., et al. 2007, *ApJS*, 170, 335
 Peebles, P. J. E., Dicke, R. H. 1968, *ApJ*, 254, 451
 Pryor, C., Meylan, G. 1993, in *ASP Conf. Proc.* 50, *Structure and Dynamics of Globular Clusters*, ed. S. Djorgovski & G. Meylan (San Francisco: ASP), 357
 Puzia, T. H., Perrett, K. M., Bridges, T., 2005, *A & A*, 434, 909
 Ricotti, M., 2002, *MNRAS*, 336, L33
 Ricotti, M. Ostriker, J. P. 2004, *MNRAS*, 352, 547
 Ricotti, M., Gnedin N. Y., Shull, J. M., 2008, *ApJ*, 685, 21
 Saitoh, T. R., Koda, J., Okamoto, T., Wada, K., & Habe, A., 2006, *ApJ*, 640, 22
 Schaerer, D. 2002, *A&A*, 382, 28
 Sokasian A., Yoshida N., Abel T., Hernquist L., Springel V., 2004, *MNRAS*, 350, 47
 Simon, J. D., Geha, M., 2007, *ApJ*, 670, 313
 Stecher T. P., Williams D. A., 1967, *ApJ*, 149, L29
 Susa, H., Kitayama, T. 2000, *MNRAS*, 317, 175
 Susa, H., Umemura, M. 2000, *MNRAS*, 316, L17
 Susa, H., Umemura, M. 2004, *ApJ*, 600, 1
 Susa, H., Umemura, M. 2006, *ApJ*, 645, L93
 Tajiri, Y., Umemura, M. 1998, *ApJ*, 502, 59
 Thoul, A. A., Weinberg, D. H., 1996, *ApJ*, 465, 608
 Tolstoy, E. et al., 2004, *ApJ*, 617, 119
 Umemura M., Ikeuchi S., 1984, *Prog. Theor. Phys.*, 72, 47
 Yoshida, N., Abel, T., Hernquist, L., Sugiyama, N., 2003, *ApJ*, 592, 645
 Yoshida, N., Omukai, K., Hernquistm L., Abel, T., 2006, *ApJ*, 663, 687